

Evolution of atomic rearrangements in deformation in metallic glassesB. S. Shang,¹ M. Z. Li,^{2,*} Y. G. Yao,^{3,†} Y. J. Lu,³ and W. H. Wang⁴¹*State Key Laboratory of Nonlinear Mechanics, Institute of Mechanics, Chinese Academy of Sciences, Beijing 100190, China*²*Department of Physics, Renmin University of China, Beijing 100872, China*³*School of Physics, Beijing Institute of Technology, Beijing 100081, China*⁴*Institute of Physics, Chinese Academy of Sciences, Beijing 100190, China*

(Received 7 January 2014; revised manuscript received 25 March 2014; published 7 October 2014)

Atomic rearrangements induced by shear stress are fundamental for understanding deformation mechanisms in metallic glasses (MGs). Using molecular dynamic simulation, the atomic rearrangements characterized by nonaffine displacements (NADs) and their spatial distribution and evolution with tensile stress in Cu₅₀Zr₅₀ MG were investigated. It was found that in the elastic regime the atomic rearrangements with the largest NADs are relatively homogeneous in space, but exhibit strong spatial correlation, become localized and inhomogeneous, and form large clusters as strain increases, which may facilitate the so-called shear transformation zones. Furthermore, initially they prefer to take place around Cu atoms which have more nonicosahedral configurations. As strain increases, the preference decays and disappears in the plastic regime. The atomic rearrangements with the smallest NADs are preferentially located around Cu atoms, too, but with more icosahedral or icosahedral-like atomic configurations. The preference is maintained in the whole deformation process. In contrast, the atomic rearrangements with moderate NADs distribute homogeneously, and do not show explicit preference or spatial correlation, acting as matrix during deformation. Among the atomic rearrangements with different NADs, those with largest and smallest NADs are nearest neighbors initially, but separating with increasing strain, while those with largest and moderate NADs always avoid to each other. The correlations in the fluctuations of the NADs confirm the long-range strain correlation and the scale-free characteristic of NADs in both elastic and plastic deformation, which suggests a universality of the scaling in the plastic flow in MGs.

DOI: [10.1103/PhysRevE.90.042303](https://doi.org/10.1103/PhysRevE.90.042303)

PACS number(s): 64.70.Q–, 62.20.F–, 71.55.Jv

I. INTRODUCTION

Metallic glasses (MGs) have many unique structural features and remarkable mechanical properties [1–4], such as high elastic strain limit, high strength, and high fracture toughness. However, the lack of plastic deformation ability is the weakness of MGs for engineering applications [1]. Because a clear structural picture of MGs is still absent, the deformation mechanism in MGs is far less understood than in crystalline counterparts [5,6].

Shear transformations are recognized as being mediated by the occurrence of local atomic rearrangements in amorphous solids [7]. Some atomic rearrangements are reversible, while others are irreversible, so that different atomic rearrangements may be involved in different local structures [8]. So far most studies have been devoted to the shear-induced irreversible atomic rearrangements and the inhomogeneous plastic response in plastic deformation and the relationship with mechanical behavior in MGs, because MGs are thought to plastically deform based on irreversible rearrangements localized in shear transformation zones (STZs). It has been found that in the plastic regime the avalanchelike plastic flow is triggered by the spontaneous irreversible atomic rearrangements [9–12]. The irreversible atomic rearrangements localized in STZs in amorphous solids extensively cooperate to produce plastic deformation, and are further organized into shear bands [13,14]. In addition, the structural geometry of the irreversible atomic rearrangements in the plastic deformation

regime exhibit fractal features, and the size of clusters involved in the irreversible atomic rearrangements has a power-law distribution [15]. Although the irreversible rearrangements in the plastic regime have been characterized significantly, the formation of STZs where the irreversible rearrangements are localized is still not clear.

In fact, the local atomic rearrangements in MGs are quite sensitive to external stress [16]. Even in the elastic deformation regime where the atomic rearrangements are supposed to be reversible, the irreversible atomic rearrangements are already found [8,17,18]. Elastic deformation could be able to induce a significant atomic rearrangement of the most unstable local structures. Such atomic rearrangements in the elastic deformation regime may be the potential STZs [8] and could be directly correlated with the formation of STZs in the plastic regime, even the nucleation and propagation of shear bands in MGs. On the other hand, as strain increases, the reversible atomic rearrangements may be transformed to be irreversible. Such transformations could be important for understanding the formation of STZs during deformation in MGs. Therefore, it is pivotal to characterize the local atomic rearrangements and investigate their evolution with strain in both elastic and plastic deformation regimes for understanding the deformation mechanism in MGs. It is also desirable to elucidate how the stress-induced local atomic rearrangements, both reversible and irreversible, evolve in the deformation process, how they interact with each other to respond to the deformation, and what their spatial distributions are. In addition, the clarification of these issues may also provide useful understanding of nucleation and propagation of shear bands in MGs.

In this work, we performed molecular dynamics (MD) simulations for CuZr MG to investigate the spatial distribution

*maozhili@ruc.edu.cn

†ygyao@bit.edu.cn

and evolution of atomic rearrangements with different non-affine displacements in tensile deformation. Three types of atoms with different degrees of atomic rearrangements were selected and analyzed. It is found that the atoms participating in different atomic rearrangements exhibit significantly different structural characteristics, spatial correlation and distribution, and evolution with increasing strain. The atoms participating in the largest atomic rearrangements are relatively localized, and form a few large clusters as strain increases. The spatial correlation of each type of atom is different. The most unstable atoms are sensitive to strain and exhibit increased pair distribution as strain increases. The correlations in the fluctuations of the nonaffine displacements show the long-range strain correlation and the scale invariance of nonaffine displacements in deformation.

This paper is organized as follows: in Sec. II we present our model and method; in Secs. III and IV results and discussion are given. Finally, a conclusion is presented in Sec. V.

II. MODEL AND METHOD

MD simulation was performed with the LAMMPS package [19] for $\text{Cu}_{50}\text{Zr}_{50}$ metallic glass with a realistic embedded-atom method potential [20]. The sample containing 96 000 atoms in a cuboid with period boundary conditions (PBCs) was first fully equilibrated at 2000 K for 1 ns, then quenched down to 50 K with the cooling rate of 1 K/ps in isothermal-isobaric (N - P - T) ensemble. [21] Finally, the quenched sample was annealed for 10 ps at 50 K. The size of the final sample is $24.75(x) \times 8.23(y) \times 8.23(z)$ nm³. In all MD simulations, the time step is 2 fs. The temperature dependence of volume and enthalpy shows the glass transition at about 740 K, and the pair distribution function confirms that as-quenched and annealed samples of $\text{Cu}_{50}\text{Zr}_{50}$ are in fully glassy states. To investigate the local atomic rearrangements, tensile stress with a strain rate of 0.0001/ps was applied to the sample along the x direction at $T = 50$ K, and along the y and z directions the pressure was controlled to be zero. PBCs were applied in all directions. In our simulations, the ten samples with different velocity seeds at 50 K were used for an ensemble average.

Figure 1 shows a typical strain(ϵ)-stress(σ) curve. The yield strain is about $\epsilon \approx 6\%$. The stress experiences three regimes as strain increases: linear elastic regime (LER) ($\epsilon = 0$ –2%), nonlinear elastic regime (NLER) ($\epsilon = 2$ –6%), and plastic regime (PR) ($\epsilon > 6\%$) as shown in Fig. 1. To characterize the local atomic rearrangements during deformation, nonaffine displacement, D_{\min}^2 , was calculated according to the following process. First, the mean-square difference $D^2(i, t, \Delta t)$ was calculated as [22]

$$D^2(i, t, \Delta t) = \frac{1}{N_i} \sum_j [\vec{r}_{ji}(t) - \gamma_i(\vec{r}_{ji}(t - \Delta t))]^2 \quad (1)$$

where $\vec{r}_{ji}(t) \equiv \vec{r}_j(t) - \vec{r}_i(t)$, and $\vec{r}_{ji}(t - \Delta t) \equiv \vec{r}_j(t - \Delta t) - \vec{r}_i(t - \Delta t)$. i denotes the central atom, and j indexes the nearest neighbors of the central atom i . N_i is the number of nearest neighbors of atom i determined by Voronoi analysis, and γ_i is the locally affine transform tensor. Δt in Eq. (1) is the time interval for atomic rearrangement and corresponds to a strain

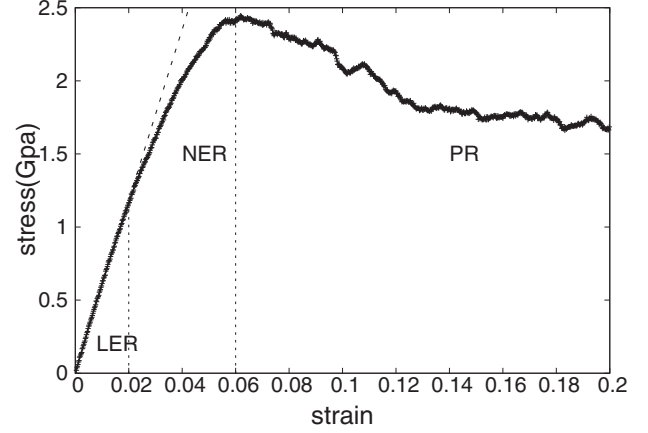


FIG. 1. Strain-stress curve in tensile deformation. Here LER, NLER, and PR represent linear elastic regime, nonlinear elastic regime, and plastic regime, respectively.

increment of 0.2% in the calculations. Using least squares method, D^2 is minimized by calculating

$$X_i = \sum_j [(\vec{r}_{ji}(t))^T (\vec{r}_{ji}(t - \Delta t))], \quad (2)$$

$$Y_i = \sum_j [(\vec{r}_{ji}(t - \Delta t))^T (\vec{r}_{ji}(t - \Delta t))], \quad (3)$$

$$\gamma_i = Y_i^{-1} \cdot X_i. \quad (4)$$

The minimized D^2 denoted by D_{\min}^2 is then the local deviation from affine deformation during the time interval of Δt . It has been demonstrated that D_{\min}^2 is a good parameter to describe the degree of local atomic rearrangements [13,15,22–24].

III. RESULT AND DISCUSSION

Figure 2(a) shows the probability distribution of D_{\min}^2 at different strains, which exhibits a peak and a typical long tail in larger D_{\min}^2 values with a power-law behavior [23]. As

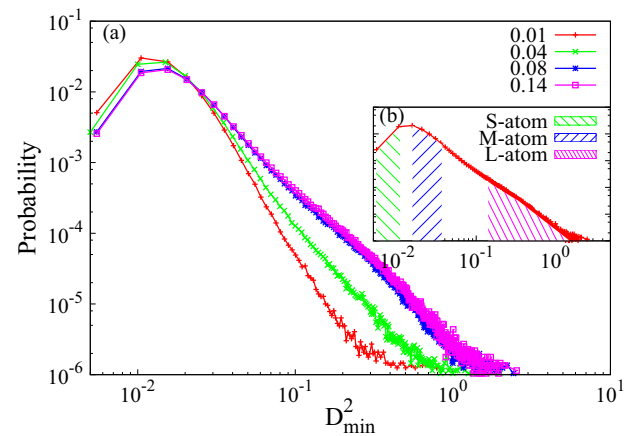


FIG. 2. (Color online) (a) Probability distribution of D_{\min}^2 at a strain of $\epsilon = 1\%$, 4%, 8%, and 14%, respectively. The inset shows the schematic of regions where three types of atoms (L , M , S) are selected.

strain increases, the distribution of smaller D_{\min}^2 gets smaller, while the long tail distribution shifts to larger D_{\min}^2 values. The distribution does not change anymore in the plastic regime. In this process, the power-law scaling exponent of the probability distribution changes from about -3.7 to about -2.0 . The peak position does not change much. As strain increases, more and more local structures experience atomic rearrangements, which significantly influences the mechanical properties of MGs. Therefore, it is desirable to know how the local atomic rearrangements, both reversible and irreversible, evolve with increasing strain and what their spatial distributions are.

To investigate the spatial distribution and evolution of local atomic rearrangements with strain, we selected three types of atoms with different values of D_{\min}^2 , 5% atoms with the smallest D_{\min}^2 (*S* atoms), 5% atoms with the largest D_{\min}^2 (*L* atoms), and 5% atoms from the middle (between 47.5% and 52.5%) of the distribution (*M* atoms) as schematically illustrated in the inset in Fig. 2. To identify the irreversible atomic rearrangements, the smallest value of D_{\min}^2 of *L* atoms in the plastic regime was employed, which is about 0.12, since the probability distribution of D_{\min}^2 of *L* atoms does not change with strain in the plastic regime. During deformation, if the value of D_{\min}^2 is larger than 0.12, the atom was assumed to experience irreversible atomic rearrangement. According to this definition, the irreversible rearrangements more or less are involved in *L* atoms.

First, we investigated pair distribution functions (PDFs) of the selected atoms at various strains. For isotropic systems, the pair distribution function is defined as

$$g(r) = \frac{1}{4\pi r^2 \rho N} \sum_{i=1}^N \sum_{j=1, j \neq i}^N \delta(r - |\vec{r}_{ij}|), \quad (5)$$

which represents the probability to find an atom at a distance r from a given atom. Here ρ is the average density of the system, N is the number of atoms, and $|\vec{r}_{ij}|$ is the distance between two atoms i and j . Figure 3 shows the PDFs of the selected atoms at various strains. The total PDFs of the sample at different strains were also presented. As shown in Fig. 3(a), the total PDF does

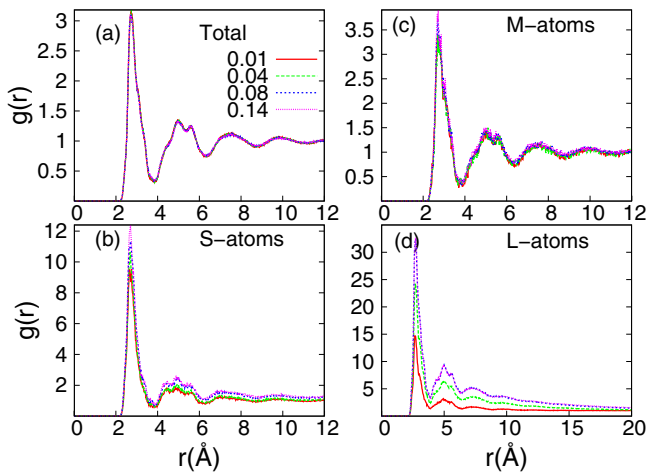


FIG. 3. (Color online) Pair distribution functions of the whole sample (a), *M* atoms (b), *S* atoms (c), and *L* atoms (d) at various strains.

not change with strain, indicating the amorphous nature of the sample under tensile stress. As strain increases, the PDF of *M* atoms does not change, either, as shown in Fig. 3(b). Moreover, the PDF intensity of *M* atoms is quite similar to that of the whole sample, indicating a homogenous distribution of *M* atoms in MGs during deformation. Therefore, *M* atoms can be considered as matrix in MGs. For *S* atoms, the PDF changes slightly with increasing strain, the intensity increasing slightly. In addition, the intensity is higher than that of the total PDF, which indicates that *S* atoms tend to get together as strain increases. Interestingly, the PDF of *L* atoms depends sensitively on strain. Both first and second peaks of the PDF are increasing with increasing strain, until finally it stops changing in the plastic regime. Even at a strain of 1%, the first peak in the PDF of *L* atoms is much higher than that of the whole sample, indicating that *L* atoms tend to form large clusters. In other words, the regions with the largest D_{\min}^2 values are relatively localized in the initial stage of deformation. As strain increases, the spatial correlation of *L* atoms becomes stronger, and the clusters formed by *L* atoms connect with each other, forming an atomic rearrangement zone in response to the external stress [1]. Note that even in the elastic regime, metallic glasses also exhibit plastic deformation [25], and some atomic rearrangements occur under stress as shown in Fig. 3(d). As strain increases, the rearrangement zones will interact with each other. Therefore, it is important to investigate the correlation of atoms with different degrees of atomic rearrangements.

We examined the composition change with strain for the three types of selected atoms. A composition ratio is defined to characterize the composition change in different type atoms as

$$R = \frac{n_{\text{Cu}}}{n_{\text{Zr}}}. \quad (6)$$

Here n_{Cu} and n_{Zr} are the number of Cu and Zr atoms in a type (*S*/*M*/*L*) of atoms, respectively. In the whole sample of $\text{Cu}_{50}\text{Zr}_{50}$ $R = 1$, so that $R > 1$ means Cu rich in a type of atom, while $R < 1$ means Zr rich in a type of atoms. Figure 4 shows the variation of the composition ratio in three types of atoms with strain. It is clearly shown that the

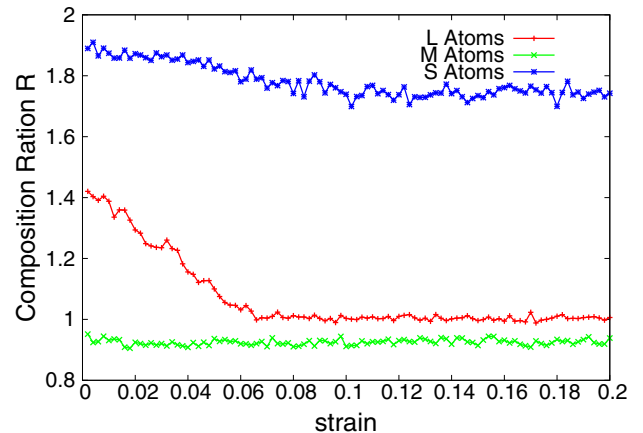


FIG. 4. (Color online) Variation of composition ratio in three types of atoms with strain.

composition ratio of M atoms is almost constant as strain increases, indicating that the composition in M atoms keeps unchanged. However, R is less than 1 and slightly deviates from the composition ratio of the whole sample, so that among M atoms, Zr is slightly rich. For S atoms, R is much larger than 1, which indicates that most S atoms are Cu. As shown in Fig. 9, in $\text{Cu}_{50}\text{Zr}_{50}$ MG almost all icosahedral clusters and icosahedral-like clusters are Cu centered, and these clusters are populated more among S atoms. It has been found that icosahedral clusters and icosahedral-like clusters are more stable [26], so that S atoms have the smallest nonaffine displacements. In contrast, the composition ratio of L atoms changes significantly with increasing strain. Initially, R is close to 1.5, larger than 1, indicating a Cu-rich composition among L atoms. As strain increases, R decreases almost linearly with strain. As the system is in the plastic regime, R reaches 1 and keeps it. This indicates that in the beginning of deformation, a large volume ($\sim 60\%$) of rearrangements occur around Cu atoms. Unlike Cu in S atoms which have more icosahedral or icosahedral-like configurations as shown in Fig. 9, in L atoms the Cu atoms are packed more loosely with their nearest neighbors, forming some nonicosahedral clusters as shown in Fig. 9, which may be quite easily deformed [26]. As strain increases, more Zr atoms are activated and evolve into the atomic rearrangements with large nonaffine displacements, so that the composition in L atoms changes and equals that of the sample in the plastic regime.

Previous work [8] on $\text{Ni}_{50}\text{Zr}_{50}$ MG also found that in elastic deformation the average fraction of Ni atoms in rearrangement clusters (similar to L atoms here) is larger than that of Zr atoms, and the composition ratio in rearrangement clusters in $\text{Ni}_{50}\text{Zr}_{50}$ is close to 1.5, too, similar to the case of $\text{Cu}_{50}\text{Zr}_{50}$ MG. This could be generic in MGs that atomic rearrangements in elastic deformation regime prefer to occur around smaller atoms. However, the reason is not so clear. We analyzed the free volume defined as $v_f = v_{\text{voronoi}} - v_{\text{atom}}$ for Cu and Zr in L atoms. Here v_{voronoi} and v_{atom} are the volume of Voronoi polyhedron and atomic volume of an atom, respectively. However, it is found that the free volume of Cu in L atoms is smaller than that of Zr in L atoms, different from the expectation [1–4].

To characterize the spatial correlation of local atomic rearrangements, a nearest-neighbor correlation index C_{ij} was employed to compare the distribution of atoms with different values of D_{\min}^2 to a statistically random distribution [27],

$$C_{ij} = \frac{p_{ij}}{p_{ij}^0} - 1 \quad (i, j = S, L, M). \quad (7)$$

Here p_{ij} is the probability of atoms of type i and type j to be the nearest neighbors in the generated sample, and p_{ij}^0 is the value for a random distribution, which is calculated by [27]

$$p_{ij}^0 = \begin{cases} \frac{2N_i N_j}{N(N-1)} & (i \neq j), \\ \frac{N_i(N_i-1)}{N(N-1)} & (i = j), \end{cases} \quad (8)$$

where N_i (N_j) is the number of atoms of type i (j) and N is the total number of atoms in the structural model. A positive value of C_{ij} indicates the strong correlation between i type atoms and j type atoms. Moreover, the more positive, the more the two types of atoms tend to be nearest neighbor. A negative

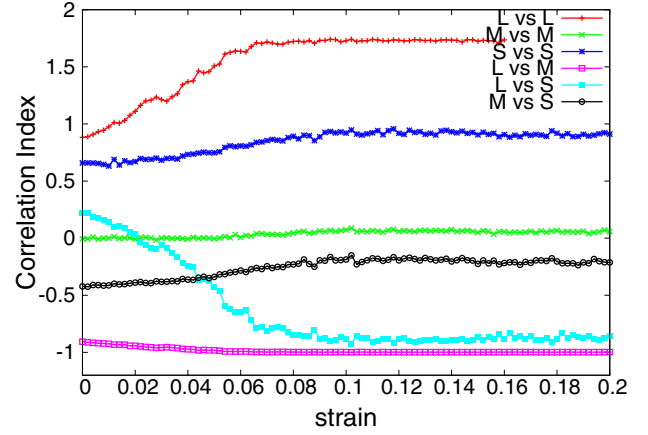


FIG. 5. (Color online) Variation of correlation index C_{ij} ($i, j = L, M, S$) with strain among L , M , and S atoms, respectively.

value of C_{ij} indicates that the two types of atoms are unlikely to be nearest neighbors. $C_{ij} \approx 0$ means that the two types of atoms are uncorrelated in materials.

Figure 5 shows the variation of the correlation index C_{ij} between three types of selected atoms as strain increases. It is clearly shown that C_{LL} is positive and increases with increasing strain, finally reaching a constant value in the plastic regime. This indicates that L atoms tend to be nearest neighbors, and the tendency becomes stronger, consistent with the above PDF analysis. Such a strong tendency of being nearest neighbors results in the clustering of L atoms. For M atoms, C_{MM} is almost zero, showing no correlation among M atoms and indicating a random distribution of M atoms. The behavior of C_{SS} is similar to C_{LL} . However, the correlation between S atoms is much weaker than between L atoms. On the other hand, C_{LM} between L atoms and M atoms is negative, and does not change much with strain, which indicates that L atoms and M atoms are distributed separately in space, and this separation is maintained during the deformation. For M atoms and S atoms, C_{MS} is negative, but approaches zero as strain increases. Initially, M atoms and S atoms tend to be separate. In the plastic regime, their spatial distributions become more random. As shown in Fig. 5, C_{LS} between L atoms and S atoms changes significantly with strain. Initially, L atoms and S atoms exhibit positive correlation, indicating that they are the nearest neighbors with each other. However, this situation changes as the deformation enters into the nonlinear elastic regime, C_{LS} becoming more and more negative until reaching a constant value in the plastic regime. This finally leads to the separation of L atoms and S atoms during deformation. The different spatial correlations of L and S atoms lead to their different spatial distribution, which might induce the formation of STZs, and even further the nucleation of shear bands [8,17]. In this process, L atoms will collect together, form big clusters, and reach the plastic flow state. Note that in the plastic regime, the material reaches a self-organized critical state [15], and the correlation does not change. Note also that, for LL and SS , a value of correlation index indicates a collective motion of atoms.

To further investigate the spatial distribution of three types of atoms and their evolution with strain, we analyzed the connectivity of three types of atoms, respectively. The degree of connectivity of an atom k can be defined as the number of the

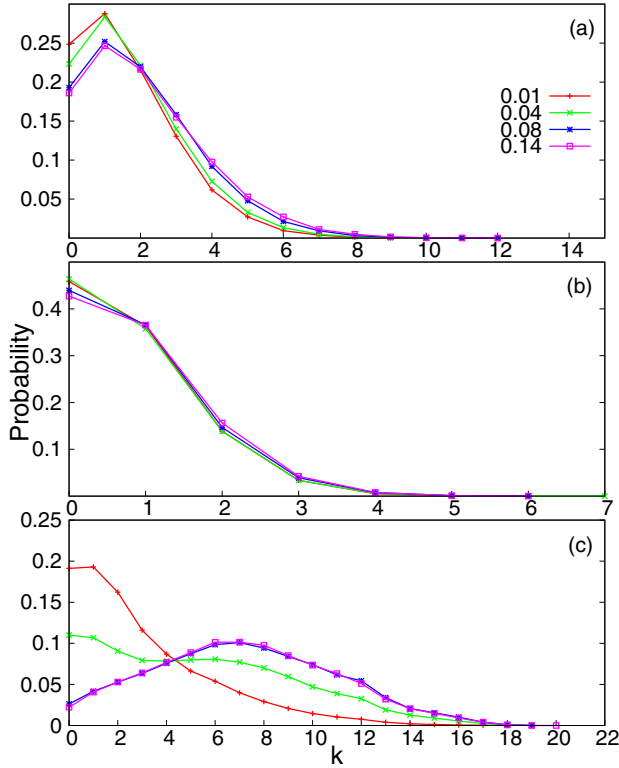


FIG. 6. (Color online) Connectivity distribution and evolution with strain for three types of selected atoms: (a) S atoms, (b) M atoms, and (c) L atoms, respectively.

same type of atoms in its nearest neighbor shell. The spread of connectivity degree is characterized by a distribution function $P(k)$, which gives the probability that an atom is connected to exactly k neighbor atoms of the same type. Figure 6 shows the distribution function of connectivity of three types of atoms and the evolution with strain. For S atoms [Fig. 6(a)], about 30% of atoms are connected with another S atom. The probability decreases drastically as the connectivity degree increases. As strain increases, the probability of $k = 2$ does not change. While the probabilities of $k = 0$ and 1 decrease, those for $k > 2$ increase. However, the distribution shape does not change much. This indicates that S atoms exhibit a certain aggregation with increasing strain. For M atoms, the probability distribution decreases monotonically with k . In addition, the distribution does not change much with strain. This is consistent with the picture of the M atoms acting as a matrix. In contrast, the probability distribution of L atoms changes significantly with strain as shown in Fig. 6(c). In the elastic regime, the distribution exhibits monotonic decrease as strain increases. Most L atoms are isolated or connected with a couple of other L atoms. As strain increases, the probabilities of small connectivities are getting lower, and those of $k > 5$ are getting more probable. In the plastic regime, the probability has a Gaussian-like distribution, and the peak is located about $k \approx 7$. As strain further increases, the probability distribution does not change anymore. The evolution of probability distribution of L atoms with strain indicates that the distribution of L atoms in space is fractal-like in elastic regime and evolves to a few large clusters in the plastic regime, which may be considered

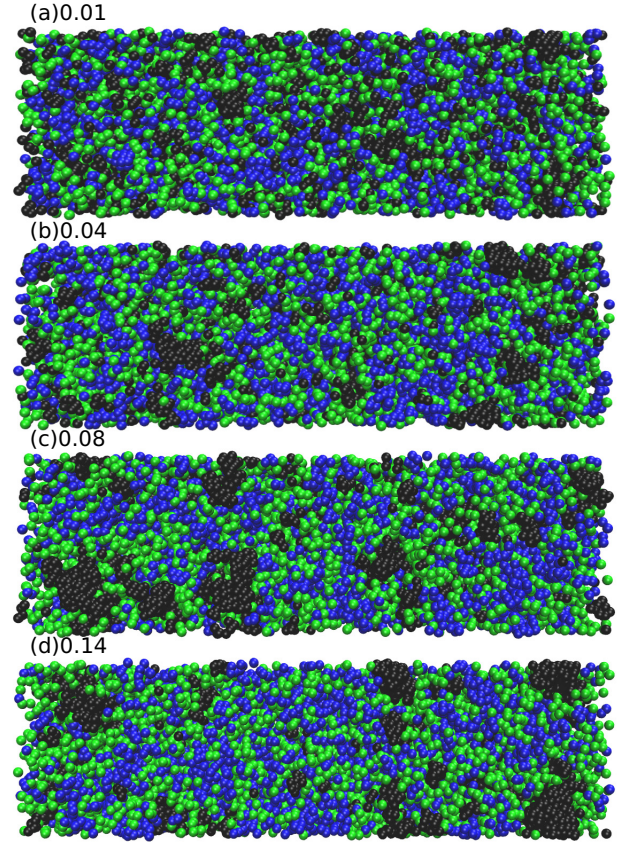


FIG. 7. (Color online) Atomistic configurations of L atoms (black), S atoms (green or light gray), and M atoms (blue or dark gray) at strain = 1% (a), 4% (b), 8% (c), and 14% (d) (top view in z direction). The box sizes are $24.99(x) \times 8.20(y) \times 8.19(z)$ nm³, $25.74(x) \times 8.10(y) \times 8.10(z)$ nm³, $26.73(x) \times 7.96(y) \times 7.95(z)$ nm³, $28.21(x) \times 7.75(y) \times 7.73(z)$ nm³, respectively.

as shear transformation zones to accommodate the external stress. Figure 7 clearly illustrates the evolution of the spatial distribution with increasing strain for L , M , and S atoms, respectively, consistent with the connectivity analysis shown in Fig. 6.

We also investigated the correlations in the fluctuations of the nonaffine displacement D_{\min}^2 defined by

$$C(\delta r, \epsilon) = \frac{\langle D_{\min}^2(r + \delta r, \epsilon) D_{\min}^2(r, \epsilon) \rangle - \langle D_{\min}^2(r, \epsilon) \rangle^2}{\langle D_{\min}^2(r, \epsilon)^2 \rangle - \langle D_{\min}^2(r, \epsilon) \rangle^2}, \quad (9)$$

where the angular brackets denote an ensemble average. Figure 8 shows the correlation function $C_{D_{\min}^2}$ as a function of distance at different strains. It can be seen that the correlation function decays with distance and roughly follows a power-law behavior beyond the nearest-neighbor distance, $C \sim \delta r^{-\beta}$. For different strains, the exponent β is different. As strain increases, the exponent is decreasing and the correlation function may be converged in the plastic flow regime as shown in Fig. 8. We roughly estimated the exponent of the converged curve and $\beta \approx 1.50 \pm 0.03$ was obtained, which is close to the values measured in colloidal glass [13]. As shown in Fig. 8, the correlation functions exhibit an enhancement in the range 3–4 Å which corresponds to the range of the

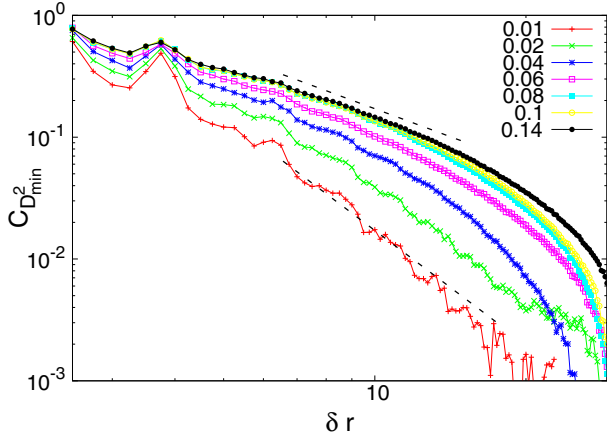


FIG. 8. (Color online) Correlations in the fluctuations of nonaffine displacements at different strains (dashed black line for line slope).

nearest-neighbor shell as indicated in Fig. 3, especially in elastic regime. As strain increases, the magnitude becomes smaller. These results indicate that the correlation of D_{\min}^2 among the nearest neighbors is significant, especially in the elastic regime.

Our results also indicate the existence of long-range strain correlations in metallic glasses, even in elastic deformation regime. The long-range strain correlation has been established in colloidal glasses and MGs but in the plastic flow regime, where the long-range elastic interactions between STZs lead to scale-free deformation of both colloidal glasses and MGs in plastic deformation [13,15]. In MGs there also exist long-range strain correlations between the nonaffine displacements in the elastic regime, indicating the scale invariance of the nonaffine displacement in both elastic and plastic regimes. However, the scaling exponent is different in different regimes as shown in Fig. 8. On the other hand, the scale invariance of the nonaffine displacements observed in MGs together with that in colloidal glasses suggests a universality of the scaling in the plastic flow and relaxation of amorphous materials.

IV. DISCUSSION

Previous numerical findings indicate that the response of MGs to shear deformation is significantly inhomogeneous [1,24,26]. Here it can be seen that the inhomogeneous deformation is mostly in the plastic deformation regime where the distribution of the irreversible atomic rearrangements localized in STZs is inhomogeneous. In elastic regime, however, the distribution of the irreversible atomic rearrangements is relatively homogeneous. In fact, in the linear elastic regime, although irreversible rearrangements occur, STZs are not formed. The occurrence of the irreversible rearrangements in the linear elastic regime could be regarded as the potential STZs or the nucleation of STZs [18]. In the nonlinear elastic regime, some isolated STZs have been observed, localized and inhomogeneous, which indicates that even in the elastic regime, plastic deformation may be induced in the most unstable local structures [25,28]. Therefore, with increasing strain, MGs experience a transformation from homogeneous deformation to inhomogeneous deformation. This might result

from the strong correlation among L atoms. Such a strong correlation leads L atoms to aggregate and form the so-called STZs, so that plastic flow may be further facilitated.

It is interesting that the spatial distribution of L atoms and its evolution with strain are similar to that of the most mobile particles characterized in dynamical heterogeneity in supercooled liquids. It has been found that the relaxation time of the most mobile particles is significantly shorter than that of the average particle [29]. Moreover, the most mobile particles are found to form stringlike structures and exhibit cooperative motion, which may be responsible for the β relaxation in supercooled liquids [30]. The stringlike structures of mobile particles in supercooled liquids are similar to the structures formed by L atoms in the elastic regime as shown in Fig. 6(a) where most L atoms are connected with another one or two L atoms. Such a stringlike structure is much easier to facilitate significant atomic rearrangements under small external stress in the elastic regime. On the other hand, it is found that the relaxation dynamics on the time scale of the α relaxation corresponds to a small number of crossings from one metabasin to a neighboring one, and involves a collective motion of the mobile particles with size $\sim O(40)$, forming a relatively compact cluster, in contrast to the stringlike motion in β relaxation [31]. This is similar to the structural configurations of L atoms in the nonlinear elastic and the plastic regimes as shown in Fig. 6(d), where L atoms form compact STZs which are much larger than the size $\sim O(40)$ involved in α relaxation in supercooled liquids, responsible for the external stress. Thus, shear-induced L atoms in the elastic regime might correspond to the β relaxation, while those in the plastic regime might correspond to the α relaxation driven by shear stress. The most mobile particles in supercooled liquids exhibit strong spatial correlation [29–31], similar to L atoms, which might cause the transformation of the relaxation configuration in supercooled liquids. This might be also true in this case where L atoms also exhibit strong spatial correlation, making the structures which facilitate the irreversible rearrangements transform from stringlike to compact ones. The above comparisons might have implications for understanding both the dynamical heterogeneity in supercooled liquid and mechanical behavior in deformation in metallic glasses.

Previous studies on the soft mode analysis [32,33] and local elasticity mapping [34] suggest that the irreversible rearrangements tend to take place at soft regions. Since L atoms are mostly involved in irreversible rearrangements during deformation, the soft regions are closely related to L atoms. In contrast, S atoms are related to the hard regions. In our Voronoi analysis shown in Fig. 9, more nonicosahedral clusters are populated among L atoms than S atoms, facilitating the irreversible rearrangements during deformation. This also indicates that L atoms are more likely to participate in the soft modes. Recently, the correlation between local structures and soft modes has been examined [35]. It is found that local structures with smaller local fivefold symmetry participate more in the soft modes. The local structures with smaller local fivefold symmetry mostly correspond to the nonicosahedral and less-populated clusters, so that they are also related to L atoms in our analysis. Therefore, our results are consistent with the soft mode analysis and local elasticity mapping. However, it is still not clear whether the locations of the

irreversible events could be precisely predicted from the initial structures of disordered systems. It has been shown that the soft regions are only close to the instability and the next plastic event cannot be predicted until the glass is brought close to the instability [34]. Although the irreversible atomic rearrangements are correlated with the low shear modules [36–38], soft modes [32,33], and local atomic symmetry [35], they do not exactly correspond to the soft modes, low shear modules, or local atomic symmetries [35,39]. This might be due to the very complex and highly distorted local topology motifs in metallic glasses which could exhibit quite different dynamical and mechanical response [40].

So far, the evolution of the atomic rearrangement with strain were investigated for different types of atoms, and it has been suggested that the interaction of atomic rearrangements increases until reaching the plastic flow state. MGs have heterogeneous structure at the nanoscale [41,42], consisting of solidlike atomic clusters and liquidlike regions [42–44]. As strain increases, the distribution of atomic rearrangements reflect the dynamical response of the heterogeneous structures to the external stress [15,25,41]. This behavior may also be affected by quenching rate as glass samples were prepared [8] and loading rate [45]. So far, the effect of temperature and loading rate on flow stress in the plastic deformation regime has been extensively studied [5]. Computer simulation studies have indicated that increase of temperature makes a negative additive contribution to flow stress, while increase of loading rate gives a positive additive contribution to flow stress [46]. Thus, temperature and loading rate significantly influence the evolution of the atomic rearrangement of different types of atoms, such as the spatial and size distributions. Increase of temperature may induce more atoms to be involved into the irreversible rearrangements and reduce the flow stress, finally leading to the plastic flow. As temperature increases, the difference between L and S atoms becomes smaller, which is helpful for MGs to reach homogeneous plastic flow. On the contrary, higher loading rates could suppress the irreversible atomic rearrangements, since local structures may not have enough time to realize the irreversible rearrangements. Therefore, the cluster size formed by L atoms would be much smaller as loading rate increases, and the evolution of L atoms with increasing strain shown in Fig. 7 could also be suppressed to some extent. Therefore, temperature and loading rate can significantly influence the evolution of the atomic rearrangement of different types of atoms. On the other hand, a similar effect of temperature and loading rate on flow stress has also been observed in crystalline solids where dislocation nucleation and mobility play important roles in plastic deformation [47–49]. This indicates that temperature and loading rate might have a common effect on the mechanical properties of both disordered solids and crystalline counterparts. The understanding of the dislocation-mediated deformation mechanism in crystalline solids could shed light on the evolution of atomic rearrangements in disordered solids.

V. CONCLUSION

In summary, using molecular simulation the atomic rearrangements and spatial distribution and evolution were investigated during tensile deformation in $\text{Cu}_{50}\text{Zr}_{50}$ metallic

glass. It is found that the atomic rearrangements with different nonaffine displacements exhibit significantly different spatial distribution and evolution. Initially the atomic rearrangements with the largest nonaffine displacements are relatively localized and distributed homogeneously in space, but exhibit strong spatial correlation, and become localized and inhomogeneous and form large clusters as strain increases. Therefore, the atomic rearrangements with the largest nonaffine displacements may facilitate the so-called shear transformation zones. In contrast, the atomic rearrangements with moderate nonaffine displacements distribute homogeneously, and do not show explicit preference or spatial correlation, acting as a matrix during deformation. On the other hand, the atomic rearrangements with the largest nonaffine displacements prefer to take place around Cu atoms which have nonicosahedral configurations, not Zr atoms. As strain increases, the preference decays and disappears in the plastic regime. The atomic rearrangements with the smallest nonaffine displacements prefer to be around Cu atoms, too, but with icosahedral or icosahedral-like atomic configurations. The correlations in the fluctuations of the nonaffine displacements confirm the long-range strain correlation and the scale invariance of nonaffine displacements in deformation.

ACKNOWLEDGMENTS

This work was supported by NSF of China (Grants No. 51271195, No. 51271197, No. 11021262, No. 11174337, and No. 11225418), National Basic Research Program of China (Grant No. 2012CB937500), the MOST Project of China (Grants No. 2014CB920903, No. 2015CB856800), and the Specialized Research Fund for the Doctoral Program of Higher Education of China (Grant No. 20121101110046). M.Z.L. was also supported by NCET-11-0498.

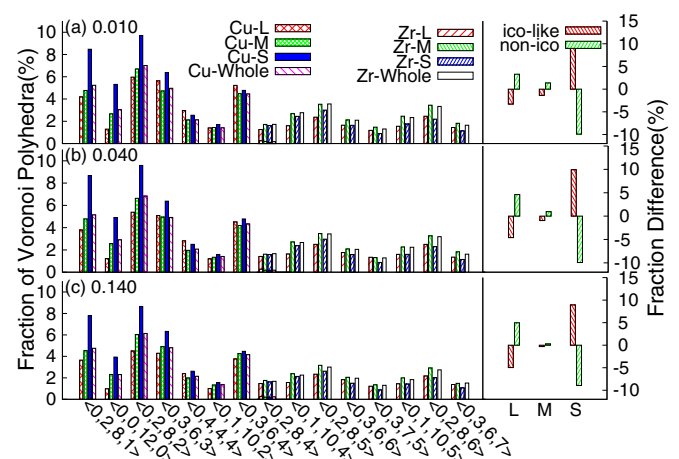


FIG. 9. (Color online) Left panel: Fractions of main populated Voronoi clusters in L , M , S , and all atoms at various strains respectively. Different colors and different patterns denote L , M , and S types of atoms, respectively. Right panel: Fraction difference of icosahedral-like (ico-like) and nonicosahedral (non-ico) clusters in L , M , and S atoms with respect to those in the whole samples, respectively.

APPENDIX: VORONOI ANALYSIS

To examine the local structures and the evolution with strain, the Voronoi tessellation method was employed [50]. In Voronoi tessellation, a local atomic cluster can be characterized by the Voronoi index, $\langle n_3, n_4, n_5, n_6, \dots \rangle$, where n_i ($i = 3, 4, 5, 6, \dots$) denotes the number of i -edge face of the Voronoi polyhedron. Since the probability of the faces with $i > 6$ is quite small, usually only the first four indices are considered. Figure 9 (left panel) shows the fractions of the main populated Cu-centered and Zr-centered clusters in L , M , and S atoms at various strains, respectively. The average fractions of these clusters in whole samples were also presented for comparison. According to previous studies, [27,37] $\langle 0,0,12,0 \rangle$, $\langle 0,1,10,2 \rangle$, $\langle 0,2,8,1 \rangle$, $\langle 0,2,8,2 \rangle$, and $\langle 0,3,6,3 \rangle$ are considered as icosahedral or icosahedral-like, and the remaining can be treated as nonicosahedral clusters, so that as shown in Fig. 9 most icosahedral-like clusters are Cu-centered. It is clearly shown that more icosahedral-like clusters are populated in

S atoms, especially for $\langle 0,0,12,0 \rangle$. This is consistent with previous studies [26]. To quantify it, we compared the fraction difference of icosahedral-like and nonicosahedral clusters in L , M , and S atoms with respect to those in all atoms, as shown in Fig. 9 (right panel). It is clear that in S atoms, the icosahedral-like clusters are much more than the average population, while the nonicosahedral clusters is much less than the average population. The fraction difference in S atoms slightly decreases in the plastic regime. In L atoms, however, the situation is reversed, and the fraction difference becomes larger as strain increases. For M atoms, the populations of icosahedral-like and nonicosahedral clusters are quite close to the average. Therefore, to compare L and S atoms, much more icosahedral-like clusters are populated in S atoms while more nonicosahedral clusters are populated in L atoms. The opposite population of icosahedral-like and nonicosahedral clusters in L and S atoms is closely related to the different mechanical response and evolution of L and S atoms during deformation.

-
- [1] C. A. Schuh, T. C. Hufnagel, and U. Ramamurty, *Acta Mater.* **55**, 4067 (2007).
- [2] M. Chen, *Annu. Rev. Mater. Res.* **38**, 445 (2008).
- [3] W. H. Wang, *Prog. Mater. Sci.* **57**, 487 (2012).
- [4] C. Byrne and M. Eldrup, *Science* **321**, 502 (2008).
- [5] D. Rodney, A. Tanguy, and D. Vandembroucq, *Modell. Simul. Mater. Sci. Eng.* **19**, 083001 (2011).
- [6] M. Falk and C. Maloney, *Eur. Phys. J. B* **75**, 405 (2010).
- [7] F. Delogu, *J. Alloys. Compd.* **513**, 251 (2012).
- [8] F. Delogu, *Intermetallics* **19**, 86 (2011).
- [9] C. Maloney and A. Lemaître, *Phys. Rev. Lett.* **93**, 016001 (2004).
- [10] C. E. Maloney and A. Lemaître, *Phys. Rev. E* **74**, 016118 (2006).
- [11] N. P. Bailey, J. Schiøtz, A. Lemaître, and K. W. Jacobsen, *Phys. Rev. Lett.* **98**, 095501 (2007).
- [12] E. Lerner and I. Procaccia, *Phys. Rev. E* **79**, 066109 (2009).
- [13] V. Chikkadi, G. Wegdam, D. Bonn, B. Nienhuis, and P. Schall, *Phys. Rev. Lett.* **107**, 198303 (2011).
- [14] R. Dasgupta, H. G. E. Hentschel, and I. Procaccia, *Phys. Rev. Lett.* **109**, 255502 (2012).
- [15] H. Peng, M. Li, B. Sun, and W. Wang, *J. Appl. Phys.* **112**, 023516 (2012).
- [16] C. L. Rountree, D. Vandembroucq, M. Talamali, E. Bouchaud, and S. Roux, *Phys. Rev. Lett.* **102**, 195501 (2009).
- [17] Y. Zhang, N. Mattern, and J. Eckert, *Acta Mater.* **59**, 4303 (2011).
- [18] F. Delogu, *Intermetallics* **17**, 688 (2009).
- [19] <http://lammmps.sandia.gov>
- [20] M. Mendeleev, R. Ott, M. Heggen, M. Feuerebacher, M. Kramer, and D. Sordelet, *J. Appl. Phys.* **104**, 123532 (2008).
- [21] S. Nosé, *J. Chem. Phys.* **81**, 511 (1984).
- [22] M. L. Falk and J. S. Langer, *Phys. Rev. E* **57**, 7192 (1998).
- [23] B. Utter and R. P. Behringer, *Phys. Rev. Lett.* **100**, 208302 (2008).
- [24] H. L. Peng, M. Z. Li, and W. H. Wang, *Phys. Rev. Lett.* **106**, 135503 (2011).
- [25] J. Ye, J. Lu, C. Liu, Q. Wang, and Y. Yang, *Nat. Mater.* **9**, 619 (2010).
- [26] J. Ding, Y. Cheng, and E. Ma, *Appl. Phys. Lett.* **101**, 121917 (2012).
- [27] M. Li, C. Z. Wang, S. G. Hao, M. J. Kramer, and K. M. Ho, *Phys. Rev. B* **80**, 184201 (2009).
- [28] Z. Wang, P. Wen, L. Huo, H. Bai, and W. Wang, *Appl. Phys. Lett.* **101**, 121906 (2012).
- [29] W. Kob, C. Donati, S. J. Plimpton, P. H. Poole, and S. C. Glotzer, *Phys. Rev. Lett.* **79**, 2827 (1997).
- [30] C. Donati, J. F. Douglas, W. Kob, S. J. Plimpton, P. H. Poole, and S. C. Glotzer, *Phys. Rev. Lett.* **80**, 2338 (1998).
- [31] G. A. Appignanesi, J. A. Rodriguez Fris, R. A. Montani, and W. Kob, *Phys. Rev. Lett.* **96**, 057801 (2006).
- [32] A. Widmer-Cooper, H. Perry, P. Harrowell, and D. R. Reichman, *Nat. Phys.* **4**, 711 (2008).
- [33] M. L. Manning and A. J. Liu, *Phys. Rev. Lett.* **107**, 108302 (2011).
- [34] M. Tsamados, A. Tanguy, C. Goldenberg, and J.-L. Barrat, *Phys. Rev. E* **80**, 026112 (2009).
- [35] M. Li, *J. Mater. Sci. Technol.* **30**, 551 (2014).
- [36] K. Maeda and S. Takeuchi, *Philos. Mag. A* **44**, 643 (1981).
- [37] Y. Cheng and E. Ma, *Prog. Mater. Sci.* **56**, 379 (2011).
- [38] Y. Fan, T. Iwashita, and T. Egami, *Phys. Rev. E* **89**, 062313 (2014).
- [39] M. Mosayebi, P. Ilg, A. Widmer-Cooper, and E. Del Gado, *Phys. Rev. Lett.* **112**, 105503 (2014).
- [40] A. Hirata, L. Kang, T. Fujita, B. Klumov, K. Matsue, M. Kotani, A. Yavari, and M. Chen, *Science* **341**, 376 (2013).
- [41] H. Wagner, D. Bedorf, S. Kuchemann, M. Schwabe, B. Zhang, W. Arnold, and K. Samwer, *Nat. Mater.* **10**, 439 (2011).
- [42] Y. H. Liu, D. Wang, K. Nakajima, W. Zhang, A. Hirata, T. Nishi, A. Inoue, and M. W. Chen, *Phys. Rev. Lett.* **106**, 125504 (2011).
- [43] B. A. Sun, H. B. Yu, W. Jiao, H. Y. Bai, D. Q. Zhao, and W. H. Wang, *Phys. Rev. Lett.* **105**, 035501 (2010).

- [44] J. Ding, Y. Q. Cheng, and E. Ma, *Acta Mater.* **61**, 4474 (2013).
- [45] Y. Shi and M. L. Falk, *Phys. Rev. Lett.* **95**, 095502 (2005).
- [46] J. Chattoraj, C. Caroli, and A. Lemaître, *Phys. Rev. Lett.* **105**, 266001 (2010).
- [47] Y. Fan, Y. N. Osetsky, S. Yip, and B. Yildiz, *Phys. Rev. Lett.* **109**, 135503 (2012).
- [48] T. Zhu, J. Li, A. Samanta, A. Leach, and K. Gall, *Phys. Rev. Lett.* **100**, 025502 (2008).
- [49] Y. Fan, Y. N. Osetskiy, S. Yip, and B. Yildiz, *Proc. Natl. Acad. Sci. USA* **110**, 17756 (2013).
- [50] C. H. Rycroft, G. S. Grest, J. W. Landry, and M. Z. Bazant, *Phys. Rev. E* **74**, 021306 (2006).